ACS APPLIED MATERIALS & INTERFACES

Research Article

www.acsami.org

# Benzothienobenzothiophene-Based Conjugated Oligomers as Semiconductors for Stable Organic Thin-Film Transistors

Han Yu,[†,‡] Weili Li,[†] Hongkun Tian,*[,†] Haibo Wang,[†] Donghang Yan,[†] Jingping Zhang,*[,‡] Yanhou Geng,*[,†] and Fosong Wang[†]

[†]State Key Laboratory of Polymer Physics and Chemistry, Changchun Institute of Applied Chemistry, Chinese Academy of Sciences, Changchun 130022, People's Republic of China

[‡]Faculty of Chemistry, Northeast Normal University, Changchun 130024, People's Republic of China

Supporting Information

**ABSTRACT:** Two benzothienobenzothiophene (BTBT)-based conjugated oligomers, i.e., 2,2′-bi[1]benzothieno[3,2-*b*][1]benzothiophene (**1**) and 5,5′-bis([1]benzothieno[3,2-*b*][1]benzothiophen-2-yl)-2,2′-bithiophene (**2**), were prepared and characterized. Both oligomers exhibit excellent thermal stability, with 5% weight-loss temperatures ($T_L$) above 370 °C; no phase transition was observed before decomposition. The highest occupied molecular orbital (HOMO) levels of **1** and **2** are −5.3 and −4.9 eV, respectively, as measured by ultraviolet photoelectron spectroscopy. Thin-film X-ray diffraction and atomic force microscopy characterizations indicate that both oligomers form highly crystalline films with large domain sizes on octadecyltrimethoxysilane-modified substrates. Organic thin-film transistors with top-contact and bottom-gate geometry based on **1** and **2** exhibited mobilities up to 2.12 $cm^2/V{\cdot}s$ for **1** and 1.39 $cm^2/V{\cdot}s$ for **2** in an ambient atmosphere. **1**-based devices exhibited great air and thermal stabilities, as evidenced by the slight performance degradation after 2 months of storage under ambient conditions and after thermal annealing at temperatures below 250 °C.

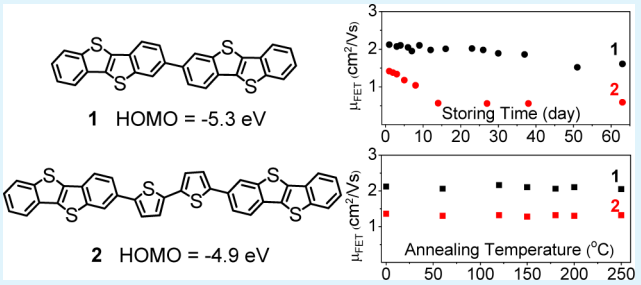


**KEYWORDS:** *benzothienobenzothiophene, conjugated oligomers, organic semiconductors, organic thin-film transistors, field-effect mobility*

## 1. INTRODUCTION

Organic thin-film transistors (OTFTs) have attracted much interest for their application in electronic devices such as radio-frequency identification tags, driving circuits of flexible displays, and low-cost memories and sensors.[1,2] In recent years, significant progress has been made in the development of organic semiconductors (OSCs) as well as fabrication techniques for high performance OTFTs.[3,4] Various OSCs with field-effect mobility ($\mu_{FET}$) exceeding 1 $cm^2/V{\cdot}s$, higher than that of amorphous silicon, have been reported.[5−23] However, for practical applications of OTFTs, it is still a great challenge to develop OSCs with high $\mu_{FET}$ as well as good air and thermal stabilities.

The recently introduced thienoacenes are OSCs that exhibit high $\mu_{FET}$ and great stability in air.[24−26] [1]Benzothieno[3,2-*b*][1]benzothiophene (BTBT) derivatives are the simplest thienoacenes that exhibit good OTFT performance. For example, p-channel OTFTs with mobilities higher than 1 $cm^2/V{\cdot}s$ have been reported using both diphenyl-substituted BTBT (DPh-BTBT) and dialkyl-substituted BTBT as semiconductors.[14,15,22] Air-stable operation of the resulting devices is attributed to the low-lying highest occupied molecular orbital (HOMO) energy levels of BTBT-based semiconductors. However, the HOMO levels of these OSCs (for example, DPh-BTBT has a HOMO of −5.8 eV[27]) are noticeably lower than the work function of the normally used gold source electrode (≈5.1 eV).[28] This difference creates a significant contact resistance between the semiconducting layer and the source electrode, which limits the device performance, especially in the linear regime. In addition, it was reported that the device performance of BTBT-based transistors was not preserved under thermal treatments above 150 °C.[29] In order to extend new applications that require processing at high temperatures, the thermal stability of OTFTs will need to be enhanced by manipulating the molecular structures of OSCs.[30] OTFTs based on higher thienoacenes, which comprise more fused rings, usually exhibited higher HOMO levels and thermal stability; however, the synthesis of these OSCs requires more steps or sophisticated reactions, which may limit their practicality.[25]

Oligomerization of small acenes or thienoacenes is an alternative synthetic approach to obtain OSCs with large

Received: January 27, 2014
Accepted: March 17, 2014
Published: March 17, 2014

   dx.doi.org/10.1021/am500598f | ACS Appl. Mater. Interfaces 2014, 6, 5255−5262

conjugation and excellent thermal stability. This approach allows extension of the $\pi$-conjugated system through the connection of feasibly synthesized building blocks and permits tuning of the molecular frontier orbital energy levels through the choice of appropriate aromatic units.[26,31−39] BTBT is a thienoacene that can be prepared in a large quantity from commercially available materials,[40] and certain derivatives exhibit remarkably high $\mu_{FET}$.[14,15,22,29] In the current paper, we report the synthesis of two conjugated oligomers based on BTBT: 2,2′-bi[1]benzothieno[3,2-*b*][1]benzothiophene (**1**) and 5,5′-bis([1]benzothieno[3,2-*b*][1]benzothiophen-2-yl)-2,2′-bithiophene (**2**). The thermal, photophysical, and charge-carrier-transport properties for **1** and **2** are reported as well.

## 2. RESULTS AND DISCUSSION

**Synthesis.** Chart 1 and Scheme 1 depict the chemical structures and synthetic route to **1** and **2**. The key intermediate,

**Chart 1. Chemical Structures of BTBT-Based Oligomers 1 and 2**

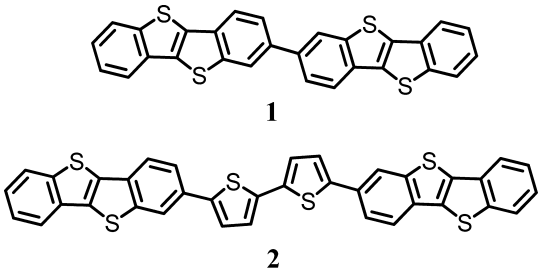


**Scheme 1. Synthetic Route to Oligomers 1 and 2**

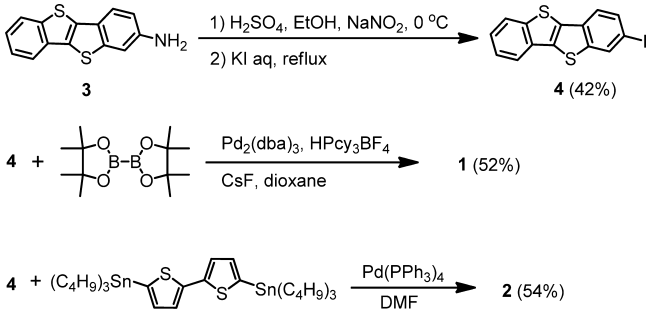


2-iodo[1]benzothieno[3,2-*b*][1]benzothiophene (**4**), was prepared from 2-amino[1]benzothieno[3,2-*b*][1]benzothiophene (**3**)[41] in a yield of 42% using a literature method.[14] Oligomer **1** was prepared by a modified Suzuki cross-coupling reaction in a yield of 52%.[42] Oligomer **2** was synthesized through a Stille coupling reaction between **4** and 5,5′-bis(tributylstannyl)-2,2′-bithiophene.[43] Both oligomers were purified using vacuum sublimation prior to characterization. The chemical structures of **1** and **2** were confirmed by elemental analysis. The structure of **1** was also validated by matrix-assisted laser desorption ionization time-of-flight (MALDI-TOF) mass spectrometry [MS; Figure S2 in the Supporting Information (SI)]. Because of their low solubility, characterization of **1** and **2** in solution was not conducted.

**Thermal and Photophysical Properties.** As shown in Figure 1, **1** and **2** exhibit good thermal stability with 5% weight-loss temperatures ($T_L$) of 371 and 450 °C, respectively, as measured by thermogravimetric analysis (TGA). No phase transition was observed for either oligomer in differential

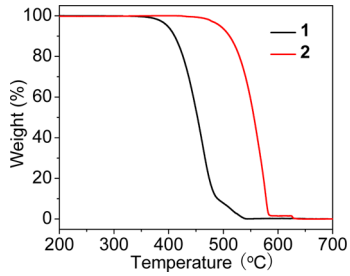


**Figure 1.** TGA plots of **1** and **2** in nitrogen with a heating rate of 10 °C/min.

scanning calorimetry scans before samples began to decompose. Thin films of **1** and **2** with a thickness of ∼50 nm were vacuum-deposited on quartz substrates for measurement of UV−vis absorption spectra. As shown in Figure 2a, oligomer **1**

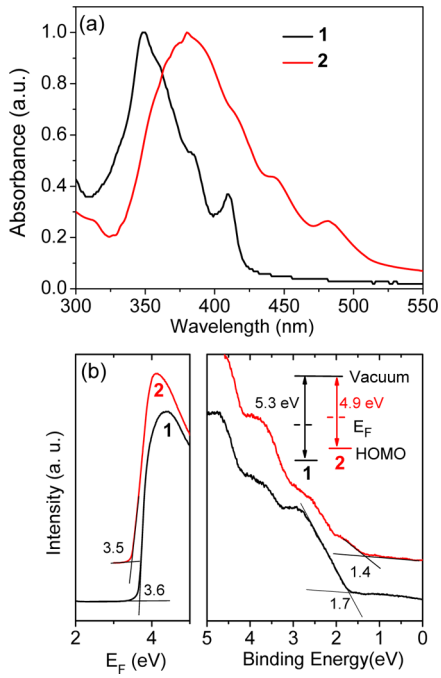


**Figure 2.** (a) Thin-film UV−vis spectra of **1** and **2**. Films with a thickness of ∼50 nm were prepared by vacuum deposition on quartz substrates. (b) Secondary electron cutoffs of the UPS (left) and onsets of the HOMO peaks (right) of **1** and **2**. The positions of onset and cutoff were estimated by linear extrapolation of the UPS profiles to the baseline.

exhibited an absorption maximum at 349 nm with the absorption onset of 425 nm, which is ∼60 nm red-shifted compared to that of C12-BTBT (365 nm), indicating an extension of $\pi$ conjugation. Oligomer **2** showed a further red-shifted absorption maximum at 380 nm along with the absorption onset of 510 nm. This is consistent with the introduction of the bithiophene segment between the two BTBT units. Optical band gaps estimated from the absorption onsets are ∼3.0 and ∼2.4 eV for **1** and **2**, respectively.

Figure 2b shows the cutoffs of the second electron tails and onsets of the HOMO peaks as measured in a vacuum by ultraviolet photoelectron spectroscopy (UPS). The ionization potentials (IPs, the absolute values of the HOMO levels relative to the vacuum level) of **1** and **2** were calculated as −5.3 and −4.9 eV, respectively, according to the formula IP = $-(E_{cutoff}$ +


dx.doi.org/10.1021/am500598f | ACS Appl. Mater. Interfaces 2014, 6, 5255−5262

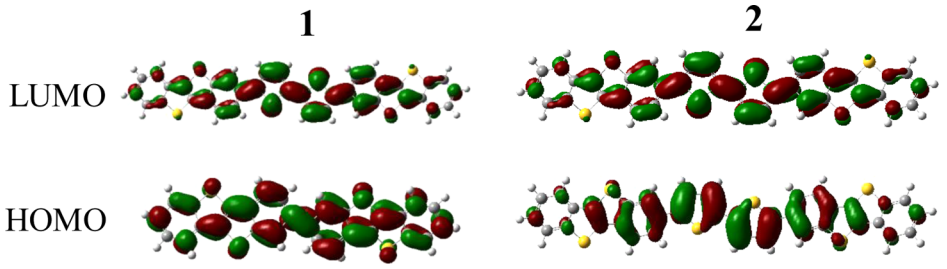


**Figure 3.** DFT-calculated (B3LYP/6-31G) molecular orbitals of **1** and **2**.

$E_{onset}$). Both values are greater than that of C12-BTBT (−6.0 eV; Figure S3 in the SI), consistent with the extension of $\pi$ conjugation in the oligomers. The IP of **1** is close to that of dinaphtho[2,3-*b*:2′,3′-*f*]thieno[3,2-*b*]thiophene (DNTT; ∼5.4 eV), while that of **2** is comparable to that of pentacene (∼5.0 eV).[27] We emphasize that the IP values of both **1** and **2** are close to the work function of gold (∼5.1 eV), which is favorable for the effective hole injection from the gold electrode to the organic semiconducting layer in OTFTs based on **1** or **2**. The lowest unoccupied molecular orbital (LUMO) levels of **1** and **2** are −2.3 and −2.5 eV, respectively, as calculated from the IP and optical band gaps.

HOMO and LUMO of **1** and **2** were modeled using density functional theory (DFT) to provide further insight into the above results and electronic structures. As shown in Figure 3, for oligomer **1**, the delocalization of the HOMO is over the entire molecule and large electron densities are found on the sulfur atoms, as in the case for the parent compound BTBT. It was proposed that the large HOMO coefficients on the sulfur atoms in BTBT is beneficial to intermolecular orbital overlap, facilitating strong intermolecular interaction.[24] However, the HOMO of **2** is primarily localized at the center part of the molecule with low electron densities on the sulfur atoms; this may be detrimental to charge transport.

**OTFT Device Performance.** OTFT devices with top-contact and bottom-gate configuration were fabricated on $SiO_2$/Si substrates to determine the semiconducting properties of **1** and **2**. Prior to deposition of the active layer, the substrates were modified with octadecyltrimethoxysilane (ODTS), according to Bao's report.[44] The thickness of the active layer was controlled at ∼30 nm. For both oligomers, several substrate temperatures ($T_{sub}$) were selected in order to attain the best device performance. The OTFT performance is summarized in Table 1. All of the devices exhibited typical p-channel OTFT properties under ambient conditions. Figure 4 shows typical output and transfer characteristics of OTFTs based on **1** and **2** at optimized $T_{sub}$. The output characteristics show standard linear and saturation regions. Importantly, the feature of injection barriers was not observed in the low-$V_D$ regime. At $T_{sub}$ = 130 °C, devices based on **1** exhibited the highest $\mu_{FET}$ of 2.12 cm$^2$/V·s with a current on/off ratio over $10^6$. Note that the mobilities of OTFTs fabricated in this condition varied in a relatively broad range (1.34−2.12 cm$^2$/V·s). We attribute this fluctuation of the mobility to the nonuniformity of the film caused by cracking (see the following discussion on the film morphology). In fact, most tested devices exhibited mobilities >1.8 cm$^2$/V·s; only a few had relatively low mobilities (1.3−1.8 cm$^2$/V·s). For oligomer **2**, the highest mobility observed was 1.39 cm$^2$/V·s at $T_{sub}$ = 190 °C. For comparison, we also fabricated OTFTs of DNTT at different $T_{sub}$ values and deposition rates. A $\mu_{FET}$ of 1.50 cm$^2$/V·s was obtained at $T_{sub}$= 60 °C (Table S1 and Figure S4 in the SI). This indicates that **1** and **2** have semiconducting properties comparable to those of DNTT. The mobility of **1**-based OTFTs is among the best reported for oligomeric semiconductors measured under ambient conditions.[7,8,26,45,46]

**Table 1. OTFT Performance of 1- and 2-Based OTFT Devices**

| | $T_{sub}$ (°C) | $\mu_{FET}$ (cm$^2$/V·s) | $V_T$ (V) | $I_{on}/I_{off}$ |
|---|---|---|---|---|
| **1** | 100 | 0.14−0.15 | −25 to −32 | $10^5$ |
| | 120 | 0.49−0.70 | −22 to −27 | $10^6$ |
| | 130 | 1.34−2.12 | −20 to −28 | $10^6$ |
| | 140 | 0.32−0.74 | −22 to −30 | $10^6$ |
| **2** | 150 | 0.20−0.22 | −10 to −13 | $10^6$ |
| | 180 | 0.68−0.88 | −18 to −22 | $10^6$ |
| | 190 | 1.34−1.39 | −20 to −22 | $10^6$ |
| | 200 | 0.73−0.79 | −22 to −27 | $10^6$ |

The air stability of the OTFTs was tested by storing the devices in an ambient atmosphere (relative humidity: 30−50%) and measuring the device performance after various durations. Parts a and b of Figure 5 show the variation of $\mu_{FET}$ and $V_T$ of **1**- and **2**-based OTFTs versus time. In the first month, the device based on **1** showed almost unchanged $\mu_{FET}$ of ca. 2.0 cm$^2$/V·s and a $V_T$ shift of less than 5 V. During the second month, the device exhibited a small decrease of $\mu_{FET}$ from about 2.0 to 1.5 cm$^2$/V·s and unchanged $V_T$. We attribute the decreased $\mu_{FET}$ to a decrease of the on-state current. The **2**-based OTFTs, however, displayed an attenuation in performance in the first 2 weeks, and $\mu_{FET}$ decreased from 1.4 to 0.6 cm$^2$/V·s with a $V_T$ shift of ∼+20 V. The low stability of OTFTs based on **2** can be rationalized by the high HOMO level of **2** (−4.9 eV). Similar phenomena were reported for the devices based on pentacene and octathiophene ($\alpha$8T), which have HOMO levels higher than −5.0 eV.[47,48] The thermal stability of the **1**-based OTFTs was studied by annealing the devices ($T_{sub}$ = 130 °C) in a glovebox at selected temperatures for 30 min. As shown in Figures 5c and S5a in the SI, with annealing temperatures below 250 °C, no obvious degradation in $\mu_{FET}$ or transfer characteristics was observed, and an increase of the off-state current was found only when the annealing temperature was greater than 120 °C. The thermal stability of the **2**-based OTFTs was also studied in the same method. $\mu_{FET}$ was maintained at ∼1.3 cm$^2$/V·s when the thermal annealing temperatures were below 250 °C (Figures 5c and S5b in the SI). Concomitant thermal stability and OTFT performance have also been found for devices based on 2,9-diphenyldinaphtho[2,3-*b*:2′,3′-*f*]thieno[3,2-*b*]thiophene (2,9-DPh-DNTT).[49,50] The synthesis of **1**, however, is much more straightforward, making it a promising semiconductor for applications that require devices having high thermal stability.


dx.doi.org/10.1021/am500598f | ACS Appl. Mater. Interfaces 2014, 6, 5255−5262

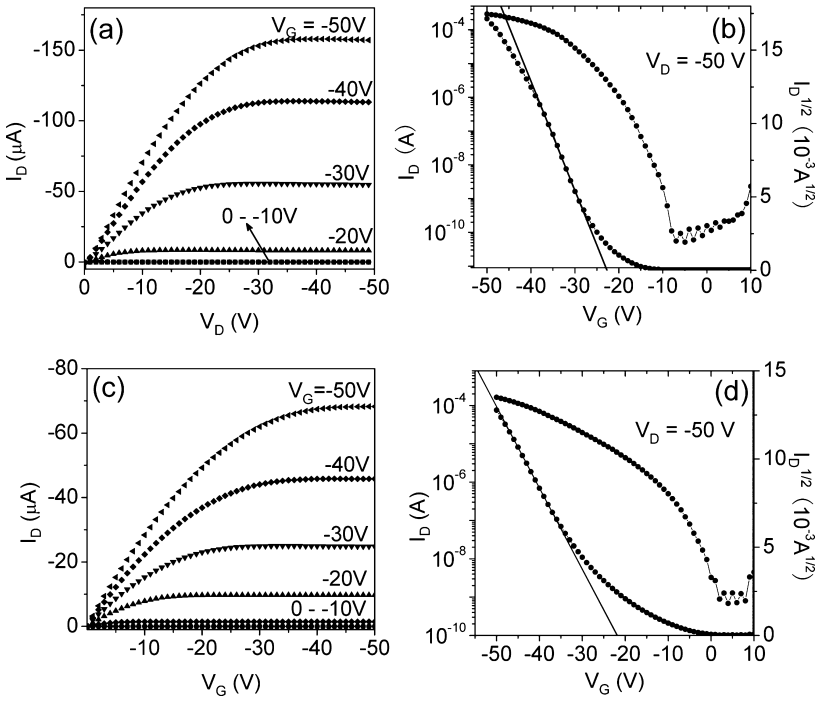


**Figure 4.** Output and transfer characteristics of OTFTs based on **1** (a and b) and **2** (c and d). The devices were fabricated at $T_{sub}$ = 130 and 190 °C for **1** and **2**, respectively.

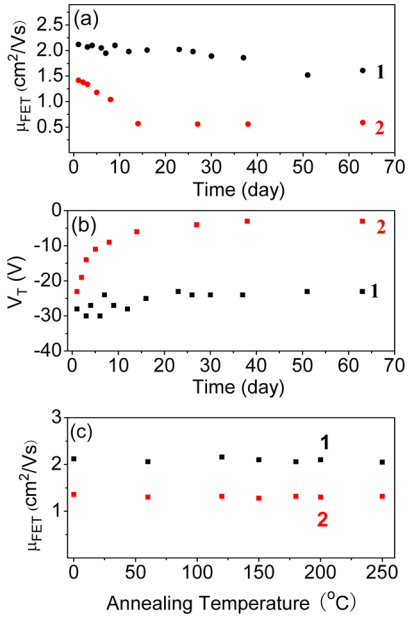


**Figure 5.** $\mu_{FET}$ (a) and $V_T$ (b) of devices based on **1** (black) and **2** (red) upon storage in ambient conditions for 2 months and $\mu_{FET}$ of devices based on **1** (black) and **2** (red) after annealing at different temperatures for 30 min (c).

**Thin-Film Microstructures.** In order to understand the $T_{sub}$-dependent device performance, thin-film microstructures of **1** and **2** were studied by X-ray diffraction (XRD) and atomic force microscopy (AFM).

Figure 6 shows AFM images of thin films of **1** and **2** prepared at different $T_{sub}$. Polycrystalline solids of both molecules grew with characteristic terraces, and the grain size of the features strongly depended on $T_{sub}$. For **1**, the grain size increased with increasing $T_{sub}$ from 1 μm at $T_{sub}$ = 100 °C to ∼10 μm at $T_{sub}$ = 130 °C, with a step height of about 2.2 nm. At the higher temperature of $T_{sub}$ = 140 °C, severe cracks were observed because of the strong crystallization of the material and the difference between the coefficients of thermal expansion of the organic and $SiO_2$/Si substrates. The thin-film morphology of **2** was investigated with $T_{sub}$ from 150 to 200 °C. At $T_{sub}$ = 190 °C, a film comprised of grains exceeding 10 μm with a step height of ∼2.8 nm was obtained. A dewetting phenomenon was observed when $T_{sub}$ was enhanced to 200 °C, likely because of a decrease in the molecules' sticking coefficient at this temperature.[48] This variation of the thin-film morphology is consistent with the $T_{sub}$-dependent device performance.

Figure 7 shows out-of-plane and in-plane thin-film XRD patterns of **1** and **2** at different $T_{sub}$ values. As shown in Figure 7a,c, the primary out-of-plane diffraction peaks of **1** and **2** were observed at $2\theta$ = 4.04 and 3.21°, corresponding to *d* spacings of 21.86 and 27.46 Å, respectively. Assuming the DFT geometry-optimized molecular lengths of 23.57 Å for **1** and 31.37 Å for **2**, the molecules contact the substrate with a title angle of about 22 and 29° from the surface normal, respectively. Multiple Bragg reflections up to (007) are observed for **1**, and these peaks intensify with increasing $T_{sub}$ from 100 to 140 °C, indicating enhanced long-range order of the thin films along the surface normal.[51] A similar behavior is observed for **2**: at $T_{sub}$ = 190 °C, the film exhibited the strongest diffraction peaks. However, when $T_{sub}$ increased to 200 °C, the peaks became weak because of dewetting of the thin film.

Parts b and d of Figure 7 show the in-plane XRD patterns of **1** and **2**. Because these diffraction patterns are similar to those of BTBT- and DNTT-based films, we propose that the molecules pack in a herringbone mode in the plane parallel to the substrate and that these peaks can be assigned as (110), (020), (120), and (200).[15,16,49] Two types of molecular packing structures coexist for **1** because two sets of diffraction peaks appear at $2\theta \approx 22$ and 30°. For discussion purposes, we define the two phases as A and A*, respectively, and the peaks can be


dx.doi.org/10.1021/am500598f | ACS Appl. Mater. Interfaces 2014, 6, 5255−5262

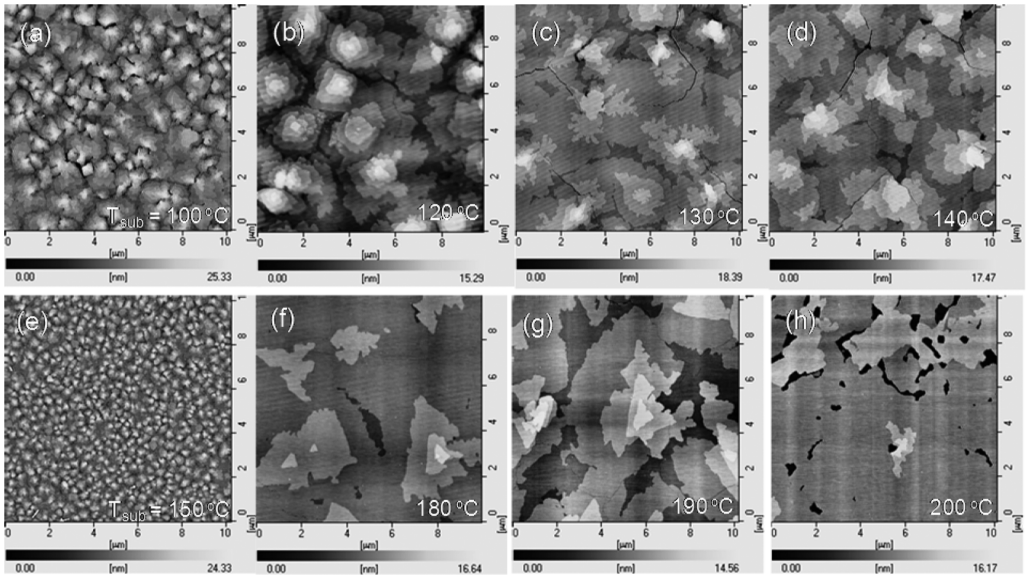


**Figure 6.** Thin-film AFM height images of **1** (a–d) and **2** (e–h) with the films prepared at different $T_{sub}$.

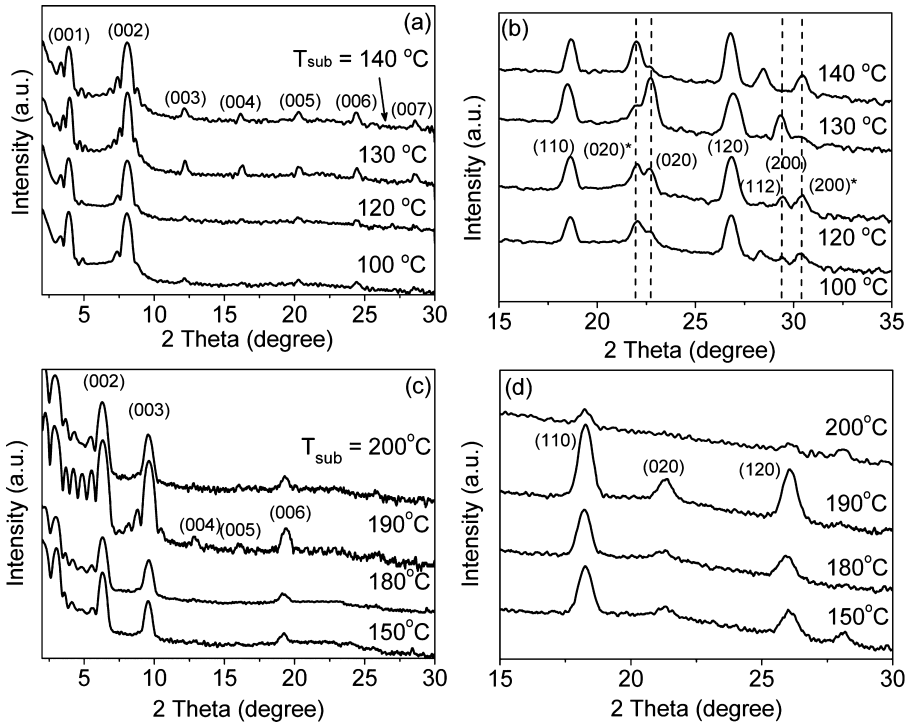


**Figure 7.** Out-of-plane (a and c) and in-plane (b and d) XRD patterns of thin films of **1** (a and b) and **2** (c and d) deposited on ODTS-modified substrates at different $T_{sub}$ values.

assigned as (020)*, (020), (200)*, and (200). Considering that **1** exhibited only one orientation along the surface normal, as evidenced in the out-of-plane XRD pattern (Figure 7a), the molecules in the two phases should pack differently in the *ab* plane, such as in herringbone angles and distances between edge-to-face-interacted molecules. After carefully analyzing the in-plane XRD patterns (Figure 7b), we propose that molecules pack in a rectangle cell in the *ab* plane and the centroid distance between edge-to-face-interacted molecules in phase A is slightly shorter than that in phase A* (see the proposed packing diagrams in Figure S6 in the SI). $T_{sub}$ has a significant effect on the composition of the two packing structures. With increasing $T_{sub}$ from 100 to 130 °C, the peak of (020) became much more intense than that of (020)*, indicating that phase A became dominant at this temperature. When $T_{sub}$ was further increased to 140 °C, the (020)* became the main peak, indicating that phase A* dominates the composition. Because the device exhibited the highest mobility at $T_{sub}$ = 130 °C, phase A is likely the high-mobility phase. This is consistent with the shorter centroid distance between edge-to-face-interacted molecules in phase A. According to the DFT calculation as shown in Figure 3, large electron densities are found on the sulfur atoms for **1**. For this type of OSCs, the intermolecular interaction through the sulfur atoms is expected to play an important role in the


dx.doi.org/10.1021/am500598f | ACS Appl. Mater. Interfaces 2014, 6, 5255–5262

intermolecular orbital overlap and consequently the carrier-transport properties.[24] The shorter centroid distance between edge-to-face-interacted molecules can induce the shorter intermolecular sulfur−$\pi$ distance and then enhance the intermolecular orbital overlap, leading to high mobility. For **2**, only one packing structure was observed. Similar to the out-of-plane diffraction patterns, the peaks became strongest at $T_{sub}$ = 190 °C.

## 3. CONCLUSION

Two oligomeric OSCs, i.e., **1** and **2**, were designed and synthesized. Both of them are capable of forming highly ordered films with large domain sizes on ODTS-modified substrates. OTFTs with mobilities up to 2.1 $cm^2/V{\cdot}s$ have been fabricated with **1** as the active layer. We emphasize that the devices were highly stable and exhibited smaller performance degradation during 2 months of storage under ambient conditions and after thermal annealing at temperatures below 250 °C. The straightforward synthesis, high field-effect mobility, and demonstrated stability make oligomer **1** a promising semiconductor for future applications.

## 4. EXPERIMENTAL SECTION

**Materials.** 5,5′-Bis(tributylstannyl)-2,2′-bithiophene and 2-amino[1]benzothieno[3,2-*b*][1]benzothiophene (**3**) were synthesized according to the literature.[41,43] *N*,*N*-Dimethylformamide (DMF) and dioxane were dried over $CaH_2$ and then freshly distilled prior to use. The other reagents and solvents were purchased and used without further purification.

*2-Iodo[1]benzothieno[3,2-b][1]benzothiophene (4).* Into an ice-cold mixture of **3** (3.00 g, 11.7 mmol), sulfuric acid (4 mL), and ethanol (80 mL), sodium nitrate (1.22 g, 17.6 mmol) in water (20 mL) was added. The mixture was stirred at 0 °C for 1 h. Then, potassium iodide (5.85 g, 35.2 mmol) in water (80 mL) was added at 0 °C, and the resulting mixture was refluxed for 4 h. The mixture was poured into aqueous sodium hydrogen sulfite. After stirring for a few minutes, the precipitate was collected by filtration, washed with methanol, and dried in a vacuum. The crude product was purified by column chromatography on silica gel with petroleum ether as the eluent to afford the product as a white solid in a yield of 42% (1.8 g). $^1$H NMR (400 MHz, $CDCl_3$): $\delta$ 8.25 (s, 1H), 7.90 (dd, $J$ = 15.2 and 7.8 Hz, 2H), 7.74 (d, $J$ = 7.7 Hz, 1H), 7.61 (d, $J$ = 7.7 Hz, 1H), 7.44 (m, 2H). Anal. Calcd for $C_{14}H_7IS_2$: C, 45.91; H, 1.93. Found: C, 45.92; H, 1.95.

*2,2′-Bi[1]benzothieno[3,2-b][1]benzothiophene (1).* Compound **4** (730 mg, 2.00 mmol), bis(pinacolato)diboron (254 mg, 1.00 mmol), $Pd_2(dba)_3$ (36 mg, 0.04 mmol), tricyclohexylphosphonium tetrafluoroborate (44.2 mg, 0.12 mmol), and cesium fluoride (2.12 g, 14.0 mmol) were added to a 50 mL round-bottomed flask containing a magnetic stir bar. The flask was evacuated and backfilled with argon three times. Then, 20 mL of degassed dioxane was added. The mixture was stirred at 80 °C for 24 h and then poured into water (100 mL). The precipitate was collected by filtration, washed with methanol, and dried in a vacuum. After sublimation twice, the product was obtained as a yellow solid in a yield of 52% (250 mg). MALDI-TOF MS (reflection mode): $m/z$ 478.0 (100%). Anal. Calcd for $C_{28}H_{14}S_4$: C, 70.26; H, 2.95. Found: C, 70.24; H, 2.96.

*5,5′-Bis([1]benzothieno[3,2-b][1]benzothiophen-2-yl)-2,2′-bithiophene (2).* To a 100 mL round-bottomed flask containing a magnetic stir bar, **4** (730 mg, 2.00 mmol), 5,5′-bis(tributylstannyl)-2,2′-bithiophene (740 mg, 1.00 mmol), and $Pd(PPh_3)_4$ (23 mg, 0.02 mmol) were added. After the flask was evacuated and backfilled with argon three times, 40 mL of DMF was added, and the reaction mixture was stirred at 90 °C for 12 h. After cooling to room temperature, the mixture was poured into saturated aqueous ammonium chloride (200 mL), and the precipitated solid was collected by filtration, washed with methanol, and dried in a vacuum. After sublimation twice, the product was obtained as an orange-yellow solid in a yield of 54% (350 mg). Anal. Calcd for $C_{36}H_{18}S_6$: C, 67.25; H, 2.82. Found: C, 67.27; H, 2.85.

**OTFT Fabrication and Characterization.** OTFTs with top-contact and bottom-gate geometry were fabricated on heavily doped silicon wafers (2 cm × 2 cm) covered with a 200-nm-thick thermally grown $SiO_2$ layer as the gate dielectric. The unit area capacitance of the gate dielectric was 17.2 $nF/cm^2$. The substrates were modified with the ODTS monolayer according to Bao's report.[44] A 30-nm-thick film of the oligomer was deposited at a pressure of $10^{-4}$ Pa and a rate of 0.3−0.4 Å/s. The gold source and drain electrodes with a thickness of 40 nm were finally deposited through a shadow mask. Eight devices were fabricated in each substrate. The channel widths ($W$) and channel lengths ($L$) of OTFTs were 3000 and 100 $\mu$m, respectively. The electrical measurements were performed with two Keithley 236 source/measure units at room temperature in an ambient atmosphere. The field-effect mobility was calculated in the saturation regime of $I_D$ using the equation

$$I_D^{sat} = (W/2L)\mu_{FET}C_i(V_G - V_T)^2$$

where $L$, $W$, and $C_i$ are the channel length, channel width, and capacitance per unit area of the dielectric layer. The air stability of the OTFTs was tested by storing the devices in an ambient atmosphere with a relative humidity of 30−50% and measuring the device performance after various durations. The devices of **1** and **2** fabricated at $T_{sub}$= 130 and 190 °C, respectively, were used for the thermal stability test. Thermal annealing of the devices was done under a nitrogen atmosphere at the selected temperature for 30 min.

## ■ ASSOCIATED CONTENT

### Supporting Information

$^1$H NMR spectrum of **4**, MALDI-TOF MS spectrum of oligomer **1**, UPS spectra of C12-BTBT, OTFT fabrication and characterization of DNTT, and transfer curves of OTFTs after annealing at different temperatures. This material is available free of charge via the Internet at http://pubs.acs.org.

## ■ AUTHOR INFORMATION

### Corresponding Authors

*E-mail: hktian@ciac.ac.cn.
*E-mail: zhangjingping66@yahoo.cn.
*E-mail: yhgeng@ciac.ac.cn.

### Notes

The authors declare no competing financial interest.

## ■ ACKNOWLEDGMENTS

This work is supported by the National Natural Science Foundation of China (Grants 51273192 and 51333006).

## ■ REFERENCES

(1) Gelinck, G.; Heremans, P.; Nomoto, K.; Anthopoulos, T. D. Organic Transistors in Optical Displays and Microelectronic Applications. *Adv. Mater.* **2010**, *22*, 3778−3798.
(2) Dimitrakopoulos, C. D.; Malenfant, P. R. L. Organic Thin Film Transistors for Large Area Electronics. *Adv. Mater.* **2002**, *14*, 99−117.
(3) Wang, C.; Dong, H.; Hu, W.; Liu, Y.; Zhu, D. Semiconducting $\pi$-Conjugated Systems in Field-Effect Transistors: A Material Odyssey of Organic Electronics. *Chem. Rev.* **2012**, *112*, 2208−2267.
(4) Mei, J.; Diao, Y.; Appleton, A. L.; Fang, L.; Bao, Z. Integrated Materials Design of Organic Semiconductors for Field- Effect Transistors. *J. Am. Chem. Soc.* **2013**, *135*, 6724−6746.
(5) Kelley, T. W.; Muyres, D. V.; Baude, P. F.; Smith, T. P.; Jones, T. D. High Performance Organic Thin Film Transistors. *Mater. Res. Soc. Symp. Proc.* **2003**, *771*, 169−178.
(6) Okamoto, H.; Kawasaki, N.; Kaji, Y.; Kubozono, Y.; Fujiwara, A.; Yamaji, M. Air-Assisted High-Performance Field-Effect Transistor with Thin Films of Picene. *J. Am. Chem. Soc.* **2008**, *130*, 10470−10471.

(7) Klauk, H.; Zschieschang, U.; Weitz, R. T.; Meng, H.; Sun, F.; Nunes, G.; Keys, D. E.; Fincher, C. R.; Xiang, Z. Organic Transistors Based on Di(phenylvinyl)anthracene Performance and Stability. *Adv. Mater.* **2007**, *19*, 3882−3887.
(8) Meng, H.; Sun, F.; Goldfinger, M. B.; Gao, F.; Londono, D. J.; Marshal, W. J.; Blackman, G. S.; Dobbs, K. D.; Keys, D. E. 2,6-Bis[2-(4-pentylphenyl)vinyl]anthracene: A Stable and High Charge Mobility Organic Semiconductor with Densely Packed Crystal Structure. *J. Am. Chem. Soc.* **2006**, *128*, 9304−9305.
(9) Kelley, T. W.; Boardman, L. D.; Dunbar, T. D.; Muyres, D. V.; Pellerite, M. J.; Smith, T. P. High-Performance OTFTs Using Surface-Modified Alumina Dielectrics. *J. Phys. Chem. B* **2003**, *107*, 5877−5881.
(10) Kaur, I.; Jia, W. L.; Kopreski, R. P.; Selvarasah, S.; Dokmeci, M. R.; Pramanik, C.; McGruer, N. E.; Miller, G. P. Substituent Effects in Pentacenes Gaining Control over HOMO−LUMO Gaps and Photooxidative Resistances. *J. Am. Chem. Soc.* **2008**, *130*, 16274−16286.
(11) Park, S. K.; Jackson, T. N.; Anthony, J. E.; Mourey, D. A. High Mobility Solution Processed 6,13-Bis(triisopropylsilylethynyl) Pentacene Organic Thin Film Transistors. *Appl. Phys. Lett.* **2007**, *91*, 063514.
(12) Llorente, G. R.; Dufourg-Madec, M.-B.; Crouch, D. J.; Pritchard, R. G.; Ogier, S.; Yeates, S. G. High Performance, Acene-Based Organic Thin Film Transistors. *Chem. Commun.* **2009**, 3059−3061.
(13) Gao, P.; Beckmann, D.; Tsao, H. N.; Feng, X.; Enkelmann, V.; Baumgarten, M.; Pisula, W.; Müllen, K. Dithieno[2,3-*d*;2′,3′-*d*′]benzo-[1,2-*b*;4,5-*b*′]dithiophene (DTBDT) as Semiconductor for High-Performance, Solution-Processed Organic Field-Effect Transistors. *Adv. Mater.* **2009**, *21*, 213−216.
(14) Takimiya, K.; Ebata, H.; Sakamoto, K.; Izawa, T.; Otsubo, T.; Kunugi, Y. 2,7-Diphenyl[1]benzothieno[3,2-*b*]benzothiophene, A New Organic Semiconductor for Air-Stable Organic Field-Effect Transistors with Mobilities up to 2.0 $cm^2$ $V^{-1}$ $s^{-1}$. *J. Am. Chem. Soc.* **2006**, *128*, 12604−12605.
(15) Izawa, T.; Miyazaki, E.; Takimiya, K. Molecular Ordering of High-Performance Soluble Molecular Semiconductors and Re-Evaluation of Their Field-Effect Transistor Characteristics. *Adv. Mater.* **2008**, *20*, 3388−3392.
(16) Yamamoto, T.; Takimiya, K. Facile Synthesis of Highly π-Extended Heteroarenes, Dinaphtho[2,3-*b*:2′,3′-*f*]chalcogenopheno-[3,2-*b*]chalcogenophenes, and Their Application to Field-Effect Transistors. *J. Am. Chem. Soc.* **2007**, *129*, 2224−2225.
(17) Kang, M. J.; Doi, I.; Mori, H.; Miyazaki, E.; Takimiya, K.; Ikeda, M.; Kuwabara, H. Alkylated Dinaphtho[2,3-*b*:2′,3′-*f*]thieno[3,2-*b*]-thiophenes (Cn-DNTTs): Organic Semiconductors for High-Performance Thin-Film Transistors. *Adv. Mater.* **2011**, *23*, 1222−1225.
(18) Kanno, M.; Bando, Y.; Shirahata, T.; Inoue, J. I.; Wada, H.; Mori, T. Stabilization of Organic Field-Effect Transistors in Hexamethylenetetrathiafulvalene Derivatives Substituted by Bulky Alkyl Groups. *J. Mater. Chem.* **2009**, *19*, 6548−6555.
(19) Weng, S.-Z.; Shukla, P.; Kuo, M.-Y.; Chang, Y.-C.; Sheu, H.-S.; Chao, I.; Tao, Y.-T. Diazapentacene Derivatives as Thin-Film Transistor Materials: Morphology Control in Realizing High-Field-Effect Mobility. *ACS Appl. Mater. Interfaces* **2009**, *1*, 2071−2079.
(20) Huang, L.; Liu, C.; Qiao, X.; Tian, H.; Geng, Y.; Yan, D. Tunable Field-Effect Mobility Utilizing Mixed Crystals of Organic Molecules. *Adv. Mater.* **2011**, *23*, 3455−3459.
(21) Li, L.; Tang, Q.; Li, H.; Yang, X.; Hu, W.; Song, Y.; Shuai, Z.; Xu, W.; Liu, Y.; Zhu, D. An Ultra Closely π-Stacked Organic Semiconductor for High Performance Field-Effect Transistors. *Adv. Mater.* **2007**, *19*, 2613−2617.
(22) Minemawari, H.; Yamada, T.; Matsui, H.; Tsutsumi, J.; Haas, S.; Chiba, R.; Kumai, R.; Hasegawa, T. Inkjet Printing of Single-Crystal Films. *Nature* **2011**, *475*, 364−367.
(23) Li, H.; Tee, B. C.-K.; Giri, G.; Chung, J. W.; Lee, S. Y.; Bao, Z. High-Performance Transistors and Complementary Inverters Based on Solution-Grown Aligned Organic Single-Crystals. *Adv. Mater.* **2012**, *24*, 2588−2591.
(24) Takimiya, K.; Shinamura, S.; Osaka, I.; Miyazaki, E. Thienoacene-Based Organic Semiconductors. *Adv. Mater.* **2011**, *23*, 4347−4370.
(25) Mori, T.; Nishimura, T.; Yamamoto, T.; Doi, I.; Miyazaki, E.; Osaka, I.; Takimiya, K. Consecutive Thiophene-Annulation Approach to π-Extended Thienoacene-Based Organic Semiconductors with [1]Benzothieno[3,2 -*b*][1]benzothiophene (BTBT) Substructure. *J. Am. Chem. Soc.* **2013**, *135*, 13900−13913.
(26) Tan, L.; Zhang, L.; Jiang, X.; Yang, X.; Wang, L.; Wang, Z.; Li, L.; Hu, W.; Shuai, Z.; Li, L.; Zhu, D. A Densely and Uniformly Packed Organic Semiconductor Based on Annelated β-Trithiophenes for High-Performance Thin Film Transistors. *Adv. Funct. Mater.* **2009**, *19*, 272−276.
(27) Yagi, H.; Miyazaki, T.; Tokumoto, Y.; Aoki, Y.; Zenki, M.; Zaima, T.; Okita, S.; Yamamoto, T.; Miyazaki, E.; Takimiya, K.; Hino, S. Ultraviolet Photoelectron Spectra of 2,7-Diphenyl[1]benzothieno-[3,2-*b*][1]benzothiophene and Dinaphtho[2,3-*b*:2′,3′-*f*]thieno[3,2-*b*]-thiophene. *Chem. Phys. Lett.* **2013**, *563*, 55−57.
(28) Kano, M.; Minari, T.; Tsukagoshi, K. Improvement of Subthreshold Current Transport by Contact Interface Modification in p-Type Organic Field-Effect Transistors. *Appl. Phys. Lett.* **2009**, *94*, 143304.
(29) Iino, H.; Kobori, T.; Hanna, J. Improved Thermal Stability in Organic FET Fabricated with a Soluble BTBT Derivative. *J. Non-Cryst. Solids* **2012**, *358*, 2516−2519.
(30) Kuribara, K.; Wang, H.; Uchiyama, N.; Fukuda, K.; Yokota, T.; Zschieschang, U.; Jaye, C.; Fischer, D.; Klauk, H.; Yamamoto, T.; Takimiya, K.; Ikeda, M.; Kuwabara, H.; Sekitani, T.; Loo, Y. L.; Someya, T. Organic Transistors with High Thermal Stability for Medical Applications. *Nat. Commun.* **2012**, *3*, 723.
(31) Murphy, A. R.; Fréchet, J. M. J. Organic Semiconducting Oligomers for Use in Thin Film Transistors. *Chem. Rev.* **2007**, *107*, 1066−1096.
(32) Mamada, M.; Nishida, J. I.; Kumaki, D.; Tokito, S.; Yamashita, Y. High Performance Organic Field-Effect Transistors Based on [2,2′]Bi[naphtho[2,3-*b*]thiophenyl] with a Simple Structure. *J. Mater. Chem.* **2008**, *18*, 3442−3447.
(33) Li, X. C.; Sirringhaus, H.; Garnier, F.; Holmes, A. B.; Moratti, S. C.; Feeder, N.; Clegg, W.; Teat, S. J.; Friend, R. H. A Highly π-Stacked Organic Semiconductor for Thin Film Transistors Based on Fused Thiophenes. *J. Am. Chem. Soc.* **1998**, *120*, 2206−2207.
(34) Sirringhaus, H.; Friend, R. H.; Li, X. C.; Moratti, S. C.; Holmes, A. B.; Feeder, N. Bis(dithienothiophene) Organic Field-Effect Transistors with a High ON/OFF Ratio. *Appl. Phys. Lett.* **1997**, *71*, 3871−3873.
(35) Sun, Y.; Ma, Y.; Liu, Y.; Lin, Y.; Wang, Z.; Wang, Y.; Di, C.; Xiao, K.; Chen, X.; Qiu, W.; Zhang, B.; Yu, G.; Hu, W.; Zhu, D. High-Performance and Stable Organic Thin-Film Transistors Based on Fused Thiophenes. *Adv. Funct. Mater.* **2006**, *16*, 426−432.
(36) Zhang, L.; Tan, L.; Hu, W.; Wang, Z. Synthesis, Packing Arrangement and Transistor Performance of Dimers of Dithienothiophenes. *J. Mater. Chem.* **2009**, *19*, 8216−8222.
(37) Laquindanum, J. G.; Katz, H. E.; Lovinger, A. J.; Dodabalapur, A. Benzodithiophene Rings as Semiconductor Building Blocks. *Adv. Mater.* **1997**, *9*, 36−39.
(38) Takimiya, K.; Kunugi, Y.; Konda, Y.; Niihara, N.; Otsubo, T. 2,6-Diphenylbenzo[1,2-*b*:4,5-*b*′]dichalcogenophenes: A New Class of High-Performance Semiconductors for Organic Field-Effect Transistors. *J. Am. Chem. Soc.* **2004**, *126*, 5084−5085.
(39) Kim, C.; Marks, T. J.; Facchetti, A.; Schiavo, M.; Bossi, A.; Maiorana, S.; Licandro, E.; Todescato, F.; Toffanin, S.; Muccini, M.; Graiff, C.; Tiripicchio, A. Synthesis, Characterization, and Transistor Response of Tetrathia-[7]-helicene Precursors and Derivatives. *Org. Electron.* **2009**, *10*, 1511−1520.
(40) Saito, M.; Osaka, I.; Miyazaki, E.; Takimiya, K.; Kuwabara, H.; Ikeda, M. One-Step Synthesis of [1]Benzothieno[3,2-*b*][1]-benzothiophene from *o*-Chlorobenzaldehyde. *Tetrahedron Lett.* **2011**, *52*, 285−288.

(41) Košata, B.; Kozmík, V.; Svoboda, J. Reactivity of [1]-Benzothieno[3,2-*b*][1]benzothiophene—Electrophilic and Metallation Reactions. *Collect. Czech. Chem. Commun.* **2002**, *67*, 645−664.
(42) Walczak, R. M.; Brookins, R. N.; Savage, A. M.; van der Aa, E. M.; Reynolds, J. R. Convenient Synthesis of Functional Polyfluorenes via a Modified One-Pot Suzuki−Miyaura Condensation Reaction. *Macromolecules* **2009**, *42*, 1445−1447.
(43) Wei, Y.; Yang, Y.; Yeh, J. M. Synthesis and Electronic Properties of Aldehyde End-Capped Thiophene Oligomers and Other $\alpha,\omega$-Substituted Sexithiophenes. *Chem. Mater.* **1996**, *8*, 2659−2666.
(44) Ito, Y.; Virkar, A. A.; Mannsfeld, S.; Oh, J. H.; Toney, M.; Locklin, J.; Bao, Z. Crystalline Ultrasmooth Self-Assembled Monolayers of Alkylsilanes for Organic Field-Effect Transistors. *J. Am. Chem. Soc.* **2009**, *131*, 9396−9404.
(45) Zhang, L.; Tan, L.; Wang, Z.; Hu, W.; Zhu, D. High-Performance, Stable Organic Field-Effect Transistors Based on *trans*-1,2-(Dithieno[2,3-*b*:3′,2′-*d*]thiophene)ethane. *Chem. Mater.* **2009**, *21*, 1993−1999.
(46) Halik, M.; Klauk, H.; Zschieschang, U.; Schmid, G.; Ponomarenko, S.; Kirchmeyer, S.; Weber, W. Relationship Between Molecular Structure and Electrical Performance of Oligothiophene Organic Thin Film Transistors. *Adv. Mater.* **2003**, *15*, 917−922.
(47) Videlot-Ackermann, C.; Ackermann, J.; Brisset, H.; Kawamura, K.; Yoshimoto, N.; Raynal, P.; Kassmi, A.; Fages, F. $\alpha,\omega$-Distyryl Oligothiophenes: High Mobility Semiconductors for Environmentally Stable Organic Thin Film Transistors. *J. Am. Chem. Soc.* **2005**, *127*, 16346−16347.
(48) Merlo, J. A.; Newman, C. R.; Gerlach, C. P.; Kelley, T. W; Muyres, D. V.; Fritz, S. E.; Toney, M. F.; Frisbie, C. D. p-Channel Organic Semiconductors Based on Hybrid Acene-Thiophene Molecules for Thin-Film Transistor Applications. *J. Am. Chem. Soc.* **2005**, *127*, 3997−4009.
(49) Yokota, T.; Kuribara, K.; Tokuhara, T.; Zschieschang, U.; Klauk, H.; Takimiya, K.; Sadamitsu, Y.; Hamada, M.; Sekitani, T.; Someya, T. Flexible Low-Voltage Organic Transistors with High Thermal Stability at 250 °C. *Adv. Mater.* **2013**, *25*, 3639−3644.
(50) Kang, M. J.; Miyazaki, E.; Osaka, I.; Takimiya, K.; Nakao, A. Diphenyl Derivatives of Dinaphtho[2,3-*b*:2′,3′-*f*]thieno[3,2-*b*]-thiophene Organic Semiconductors for Thermally Stable Thin-Film Transistors. *ACS Appl. Mater. Interfaces* **2013**, *5*, 2331−2336.
(51) Jones, B. A.; Facchetti, A.; Wasielewski, M. R.; Marks, T. J. Tuning Orbital Energetics in Arylene Diimide Semiconductors. Materials Design for Ambient Stability of n-Type Charge Transport. *J. Am. Chem. Soc.* **2007**, *129*, 15259−15278.